Supplementary information

S1. Methodology for estimation of the mass concentrations of $PM_{2.5}$ components

S1.1 Organic matter

The mass concentration of organic matter (OM) was calculated from organic carbon (OC) measurements by multiplying OC by a factor that represents the mass contributions of other elements, such as oxygen, hydrogen, and nitrogen. The OM/OC ratio varies from 1.4 to 2.2 and is expected to increase as aerosols age (El-Zanan et al., 2005). We chose a factor of 1.6 to calculate OM in Beijing following advice in the literature (Xing et al., 2013).

S1.2 Primary organic carbon

The two main sources of OC are primary (POC) emissions from fuel combustion, biomass burning, or vehicle exhaust, and secondary organic carbon (SOC) from the oxidation of volatile organic compounds (VOCs) and semi-volatile organic compounds (SVOCs). Elemental carbon (EC) is emitted directly into the atmosphere and has been used as a tracer to estimate co-emitted POC. Meanwhile, SOC can be calculated as follows (Saylor et al., 2006; Turpin and Huntzicker, 1995):

$$\mathrm{SOC} = \mathrm{OC} - \mathrm{POC} = \mathrm{OC} - \left[\left(\frac{\mathrm{OC}}{\mathrm{EC}}\right)_{\mathrm{pri}} \mathrm{EC} + b\right] , \qquad \text{(Eq. 1)}$$

where $(\mathrm{OC/EC})_{\mathrm{pri}}$ is the primary OC/EC ratio of combustion sources, and b is the primary OC emitted from non-combustion sources. These two parameters can be derived from a linear regression of OC and EC (Fig. S1). In our study, Deming regression (Deming, 1943) was applied to the lowest 10% of OC/EC values for each season to obtain the two parameters, with the slope as $(\mathrm{OC/EC})_{\mathrm{pri}}$ and the intercept as b (Fig. S1). The regression lines for the four seasons are shown in Fig. S1.

S1.3 Estimates of the OC/EC ratio in primary sources

Deming regression (1943) was applied to the lowest 10% of OC/EC samples for each season. The scatter plots and regression equations for OC against EC in each season are depicted in Fig. S1. The primary OC/EC ratios were determined to be 3.46, 2.50, 3.69, and 5.34 in spring, summer, autumn, and winter, respectively.

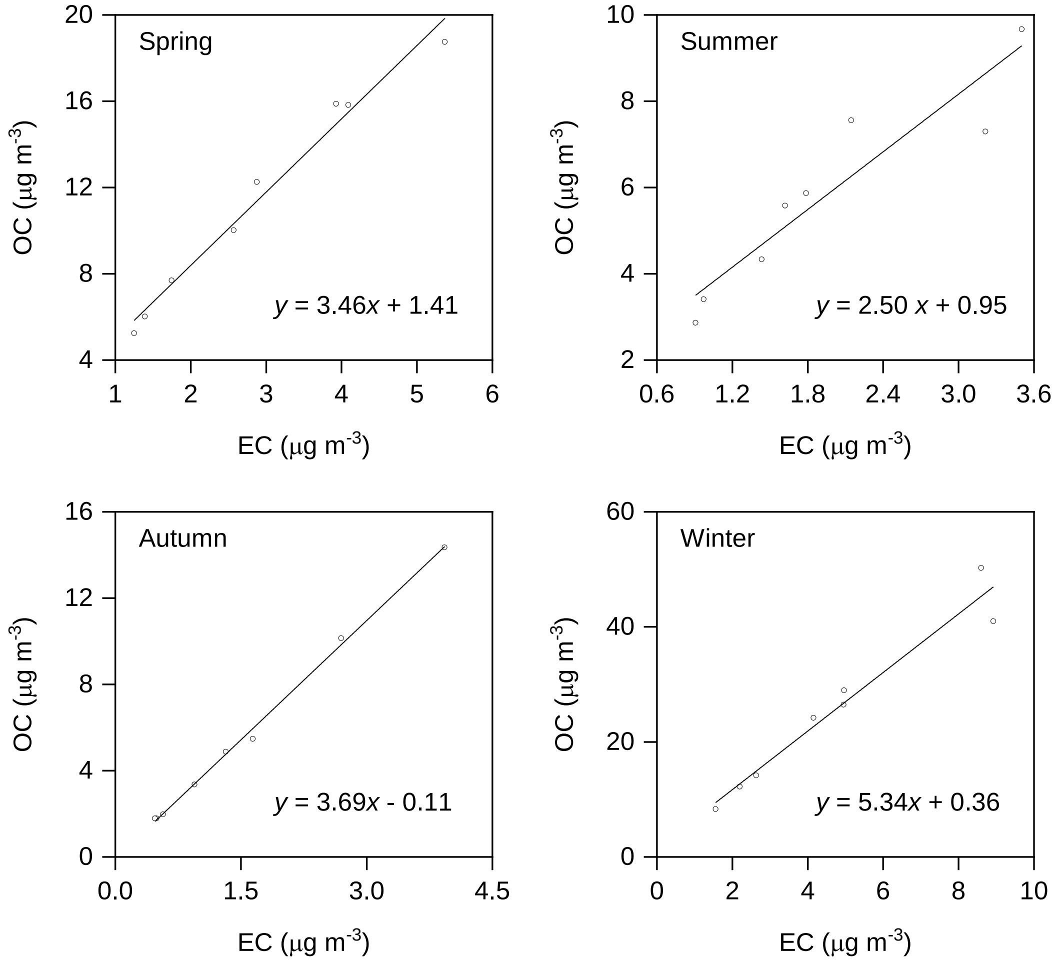

Figure S1. Scatter plots and regression equations for organic carbon (OC) against elemental carbon (EC) in each season.

S1.4 Minerals

The total mass concentration of minerals, referred to as "minerals", can be estimated by the following equation (Chan et al., 1997):

$$[\text{minerals}] = 2.2[\text{Al}] + 2.49[\text{Si}] + 1.63[\text{Ca}] + 2.42[\text{Fe}] + 1.94[\text{Ti}] \quad , \qquad \text{(Eq. 2)}$$

where [x] represents the mass concentration of species x. According to Zhang et al. (2003), on average Al accounted 7% of total mineral dust mass concentrations in North, Northwest, and West China. Mineral concentrations can thus also be estimated by Eq. 3:

$$[\text{minerals}] = [\text{Al}]/0.07 \,, \qquad \text{(Eq. 3)}$$

We calculated [minerals] with the two methods above and found no significant differences (Fig. S2). Equation 3 was therefore employed to calculate [minerals] in this study.

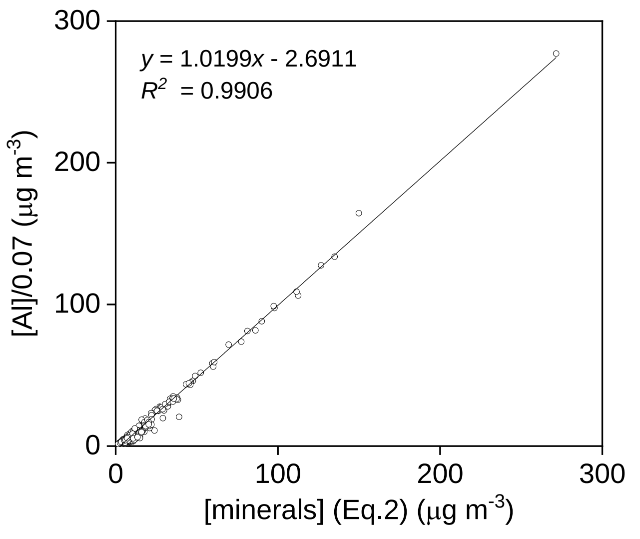

Figure S2. Comparison of the two methods for the calculation of [minerals].

S1.5 Trace element oxides

The enrichment factors (EFs) of trace element oxides (TEOs) can be used to determine whether natural or anthropogenic sources dominated our observations. The EF value of element i was defined as follows:

$$\text{EF}_i = \frac{[X_i/X_{\text{ref}}]_{\text{sample}}}{[X_i/X_{\text{ref}}]_{\text{crust}}} \,, \qquad \text{(Eq. 4)}$$

where $[X_i/X_{\text{ref}}]_{\text{sample}}$ is the mass concentration ratio of element i to the reference element in our samples and $[X_i/X_{\text{ref}}]_{\text{crust}}$ is the mass concentration ratio of element i to the reference element in average crust (Hans Wedepohl, 1995). Al was used as the reference element in this study. The EFs of each element are depicted in Fig. S3.

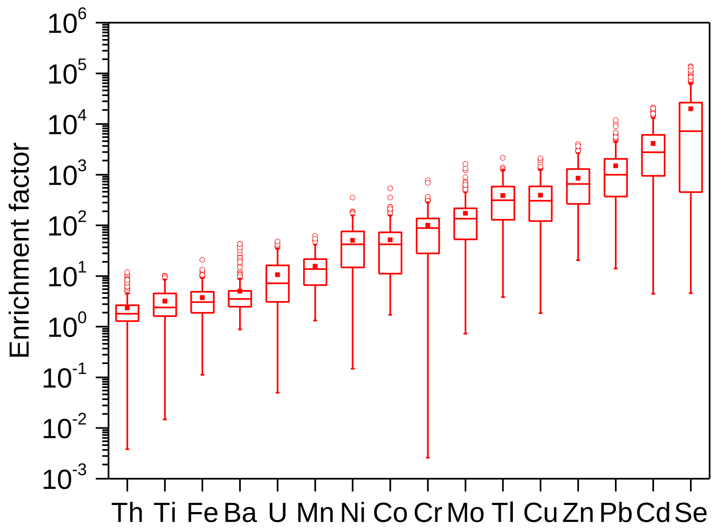

Figure S3. Elemental enrichment factors (EFs) of our samples. The boxes represent, from top to bottom, the 75th, 50th, and 25th percentiles for each element. The whiskers, solid red squares, and open red circles represent 1.5 times the interquartile range (IQR), seasonal mean values, and outlier data points, respectively.

If the EF was < 5, the element was considered to originate mainly from natural sources; if 5 < EF< 20, the element originated from both natural and anthropogenic sources; if EF > 20, the element originated mainly from anthropogenic sources. According to Zhang et al. (2013), the mass concentrations of TEOs can be estimated by multiplied a factor to represent the contribution of oxygen. For elements originating from anthropogenic sources only, a factor of 1 was applied, whereas for elements of both natural and anthropogenic origin, a factor of 0.5 was applied to represent the anthropogenic part. As multiple forms of metal oxides were identified, which were hard to quantify, a multiplicative factor of 1.3 was used when considering the metal abundance. The mass concentration of TEOs was calculated as described in Zhang et al. (2013):

$$[TEOs] = 1.3 \times [0.5 \times (Ba + Mn + U) + (Ni + Co + Cr + Mo + Tl + Cu + Zn + Pb + Cd + Se)], \qquad \text{(Eq. 5)}$$

S1.6 Aerosol water content

Aerosol water content (AWC) was calculated using the ISORROPIA-II thermodynamic model (http://isorropia.eas.gatech.edu). The Na^+–K^+–Ca^{2+}–Mg^{2+}–NH_4^+–SO_4^{2-}–NO_3^-–Cl^-–H_2O aerosol system was applied in reverse mode (Fountoukis and Nenes, 2007; Nenes et al., 1998).

S2 Results and discussion

S2.1 General description

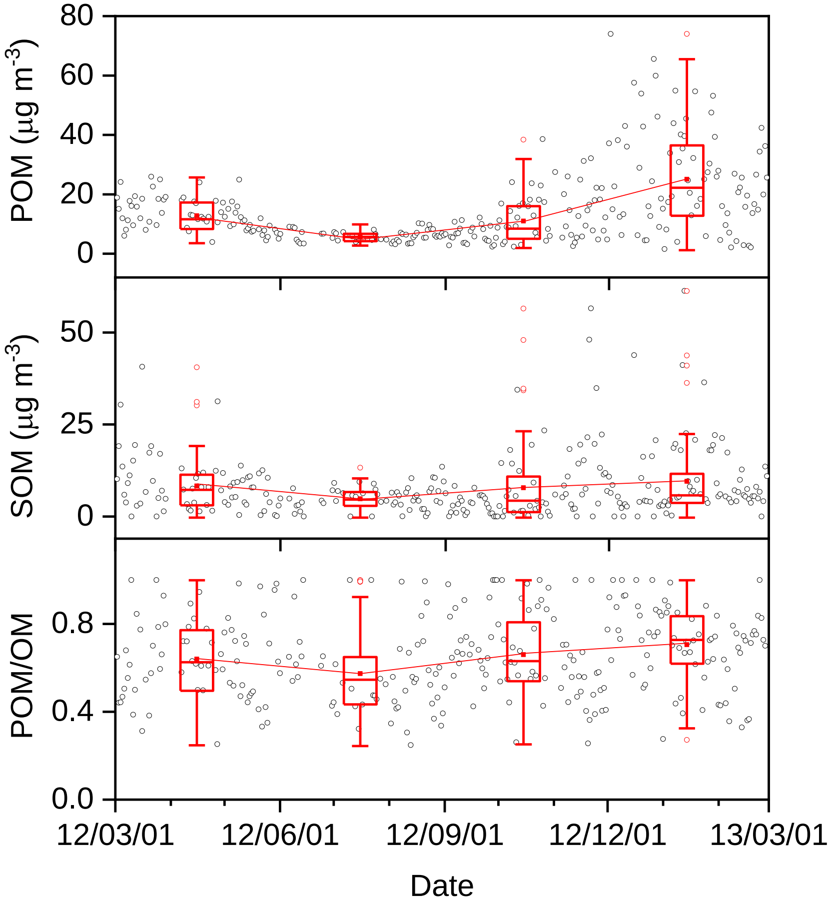

Figure S4. Time series of primary organic matter (POM), secondary organic matter (SOM), and POM/OM from March 1 2012 to February 28 2013 (open black circles). The boxes represent, from top to bottom, the 75th, 50th, and 25th percentiles for each season. The whiskers, solid red squares, and open red circles represent 1.5 times the IQR, seasonal mean values, and outlier data points, respectively.

S2.2 Sulfate formation mechanism

Sulfate can be formed through the oxidation of SO_2 by OH radicals in the gas phase (Stockwell and Calvert, 1983), through the oxidation of dissolved SO_2 by various oxidants (e.g., O_3, H_2O_2, NO_2, and O_2) in the aqueous phase (Seinfeld and Pandis, 2006), which may be transition metal ions (TMIs)-catalysed, or through heterogeneous reaction on the surface of sea-salt or dust aerosols (Gurciullo et al., 1999; Usher, 2002).

The rate of the SO_2 + OH reaction can be expressed as:

$$R_{SO_2+OH} = k_0[SO_2(g)][OH(g)] \quad , \qquad \text{(Eq. 6)}$$

where k_0 is the rate constant and [x] represents the concentration of species x. The production rate of sulfate through OH radical oxidation can be expressed as:

$$P_{OH} = \frac{3600 \times 96 \times p \times R_{SO_2+OH}}{RT} \quad , \qquad \text{(Eq. 7)}$$

where 3600 is a time conversion factor ($s\ h^{-1}$), 96 is the molar mass of SO_4^{2-} ($g\ mol^{-1}$), p is atmospheric pressure (kPa), R is the gas constant (8.31 $Pa\ m^3\ mol^{-1}\ K^{-1}$), and T is the temperature (K).

SO_2 reacts with H_2O_2, O_3, NO_2, and O_2 (TMIs-catalysed) in the aqueous phase. The rates of the four main aqueous reactions are expressed as (He et al., 2018; Seinfeld and Pandis, 2006):

$$R_{SO_2+O_3} = (k_1[SO_2 \cdot H_2O] + k_2[HSO_3^-] + k_3[SO_3^{2-}])[O_3(aq)] \quad , \qquad \text{(Eq. 8)}$$

$$R_{SO_2+H_2O_2} = \frac{k_4[H^+][HSO_3^-][H_2O_2(aq)]}{1 + K[H^+]} \quad , \qquad \text{(Eq. 9)}$$

$$R_{SO_2+NO_2} = k_5[S(IV)][NO_2(aq)] \quad , \qquad \text{(Eq. 10)}$$

$$R_{SO_2+O_2} = k_6[H^+]^{-0.74}[S(IV)][Mn(II)][Fe(III)] \qquad (pH < 4.2) \quad , \qquad \text{(Eq. 11)}$$

$$R_{SO_2+O_2} = k_7[H^+]^{0.67}[S(IV)][Mn(II)][Fe(III)] \qquad (pH > 4.2) \quad , \qquad \text{(Eq. 12)}$$

The production rate of sulfate through aqueous oxidation routes can be expressed as:

$$P_{aqu(ox_i)} = 3600 \times 96 \times R_{SO_2+ox_i} \times \frac{LWC}{\rho_{H_2O}} \quad , \qquad \text{(Eq. 13)}$$

where k_n (n = 1–7) is the rate constant of each oxidation route, $K = 13\ M^{-1}$ at 298 K, LWC is the liquid water content ($mg\ m^{-3}$), ρ_{H2O} is the density of water ($1\ kg\ L^{-1}$), and ox_i (i = O_3, H_2O_2, NO_2, and O_2) represents different oxidants.

The heterogeneous reaction rate $R_{het(ox_i)}$ can be expressed as (Jacob, 2000; Wang et al., 2012; Zheng et al., 2015):

$$R_{het(ox_i)} = k_{ox_i}[SO_2(g)] \quad , \qquad \text{(Eq. 14)}$$

where

$$k_{ox_i} = \left(\frac{d_p}{2D_i} + \frac{4}{v_i \gamma_i}\right)^{-1} S_p \quad , \qquad \text{(Eq. 15)}$$

d_p is the effective diameter of the particles (m), D_i is the gas phase molecular diffusion coefficient (m^2 s^{-1}), v_i is the mean molecular speed in the gas phase (m s^{-1}), and S_p is the aerosol surface area (m^2 m^{-3}). The uptake coefficient γ_i depends on RH:

$$\gamma_i = \left\{ \begin{array}{ll} \gamma_{low} & 0 < \mathrm{RH} \le 50\% \\ \gamma_{low} + \frac{(\gamma_{high} - \gamma_{low})(\mathrm{RH} - 0.5)}{\mathrm{RH}_{max} - 0.5} & 50\% < \mathrm{RH} \le \mathrm{RH}_{max} \\ \gamma_{high} & \mathrm{RH}_{max} < \mathrm{RH} \le 100\% \end{array} \right\} \quad \text{(Eq. 16)}$$

where γ_{low} and γ_{high} can be obtained from Wang et al. (2012) and RH_{max} is the RH at which γ reaches γ_{high}.. The rate of sulfate production via heterogeneous reactions $P_{het(ox_i)}$ can be expressed as:

$$P_{het(ox_i)} = \frac{3600 \times 96 \times p \times R_{het(ox_i)}}{RT} \ , \quad \text{(Eq. 17)}$$

S2.3 Influencing parameters

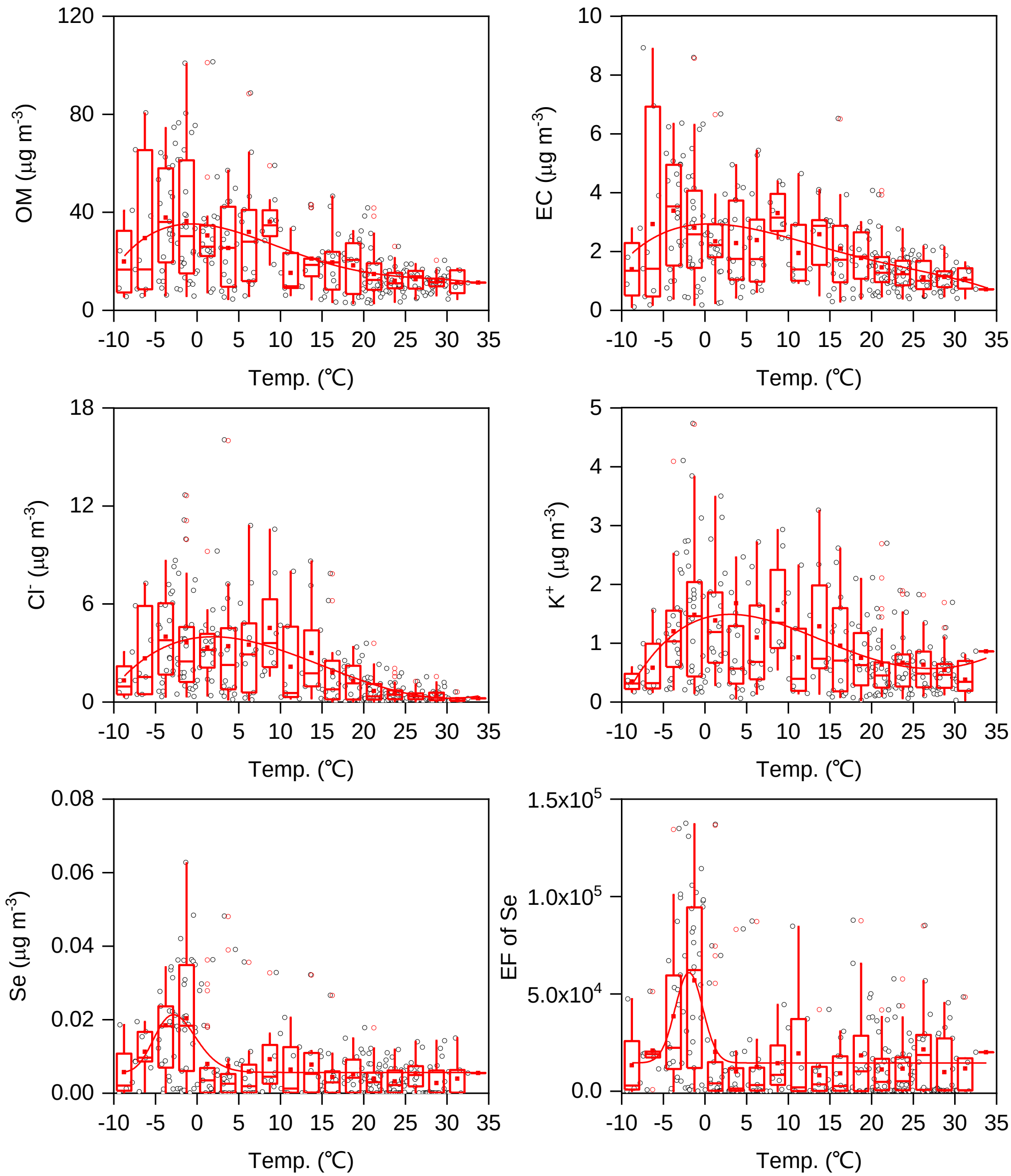

Figure S5. Plots of organic matter (OM), element carbon (EC), Cl^-, K^+, Se, and the EF of Se against temperature. The boxes represent, from top to bottom, the 75^{th}, 50^{th}, and 25^{th} percentiles in each temperature bin ($\Delta T = 2.5$ °C). The whiskers, solid red squares, and open red circles represent 1.5 times the IQR, seasonal mean values, and outlier data points, respectively. The red lines are best fits to the mean values based on either polynomial or Gaussian functions.

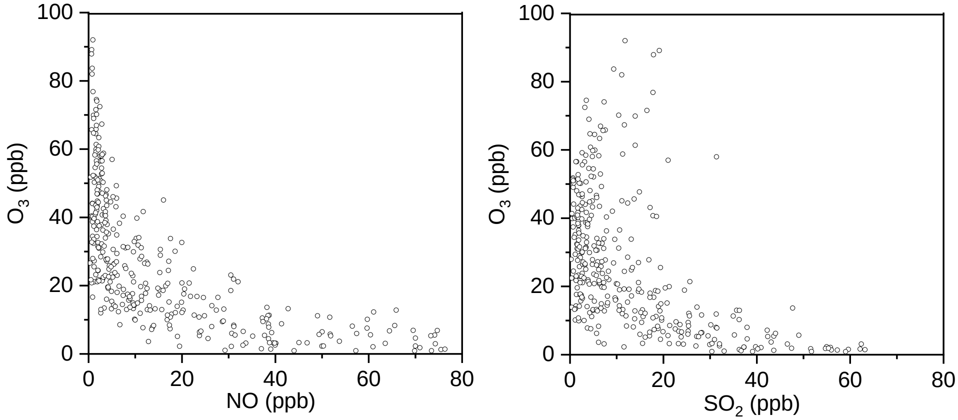

Figure S6. Plots of O_3 against the primary emission tracers NO and SO_2.

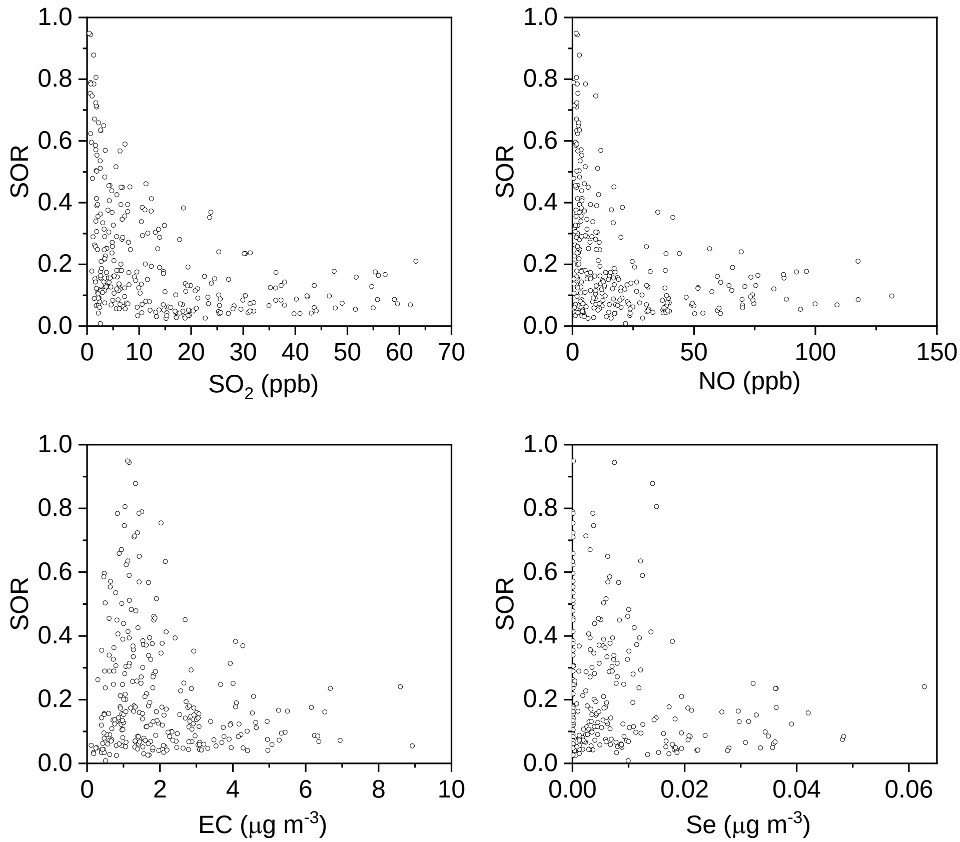

Figure S7. Plots of sulfur oxidation ratios (SORs) against the primary emission tracers SO_2, NO, EC and Se.

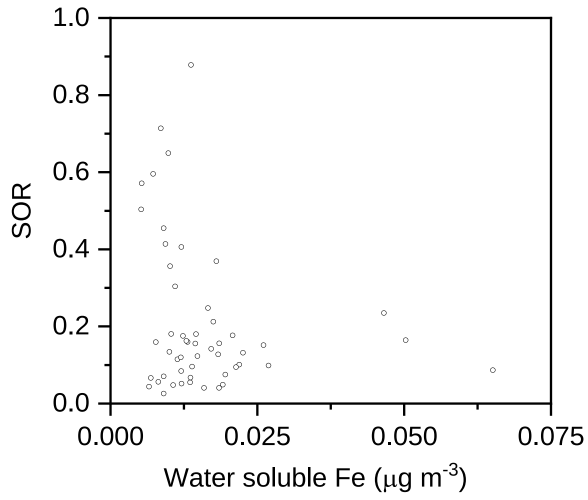

Figure S8. Plot of the SOR against water soluble Fe (54 samples selected every 6 days throughout the sampling period).

S2.4 Seasonal variations

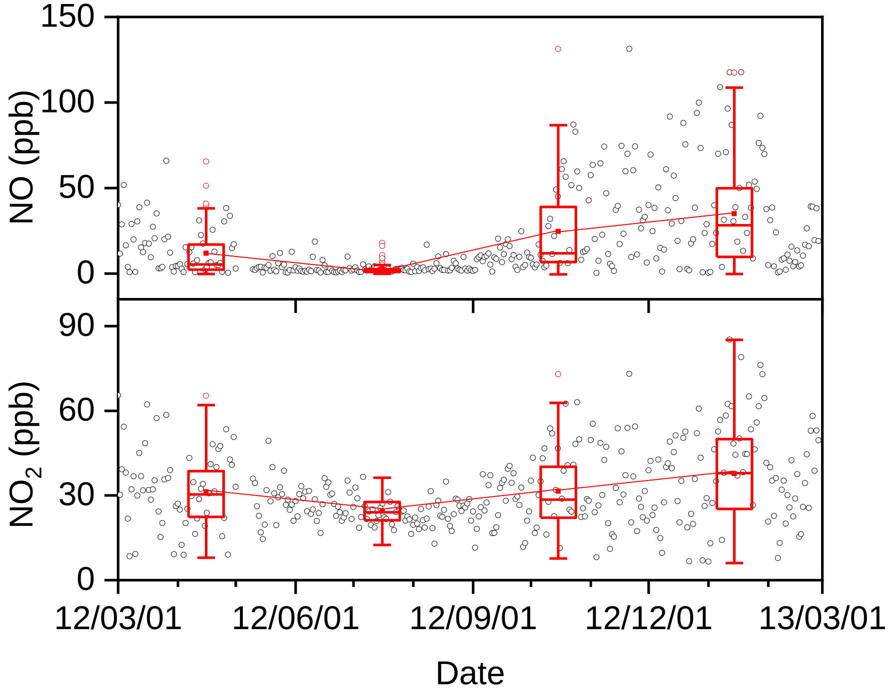

Figure S9. Time series of NO and NO_2 from March 1 2012 to February 28 2013 (open black circles). The boxes represent, from top to bottom, the 75th, 50th, and 25th percentiles for each season. The whiskers, solid red squares, and open red circles represent 1.5 times the IQR, seasonal mean values, and outlier data points, respectively.

References

Chan, Y. C., Simpson, R. W., McTainsh, G. H., Vowles, P. D., Cohen, D. D., and Bailey, G. M.: Characterisation of chemical species in $PM_{2.5}$ and PM_{10} aerosols in Brisbane, Australia, Atmos. Environ., 31, 3773-3785, https://doi.org/10.1016/S1352-2310(02)00804-X, 1997.

Deming, W. E.: Statistical adjustment of data, John Wiley & Sons, 35-63 pp., 1943.

El-Zanan, H. S., Lowenthal, D. H., Zielinska, B., Chow, J. C., and Kumar, N.: Determination of the organic aerosol mass to organic carbon ratio in IMPROVE samples, Chemosphere, 60, 485-496, https://doi.org/10.1016/j.chemosphere.2005.01.005, 2005.

Fountoukis, C., and Nenes, A.: ISORROPIA II: a computationally efficient thermodynamic equilibrium model for K^+–Ca^{2+}–Mg^{2+}–NH_4^+–Na^+–SO_4^{2-}–NO_3^-–Cl^-–H_2O aerosols, Atmos. Chem. Phys., 7, 4639-4659, https://doi.org/10.5194/acp-7-4639-2007, 2007.

Gurciullo, C., Lerner, B., Sievering, H., and Pandis, S. N.: Heterogeneous sulfate production in the remote marine environment: Cloud processing and sea-salt particle contributions, J. Geophys. Res., 104, 21719, https://doi.org/10.1029/1999jd900082, 1999.

Hans Wedepohl, K.: The composition of the continental crust, Geochim. Cosmochim. Ac, 59, 1217-1232, https://doi.org/10.1016/0016-7037(95)00038-2, 1995.

He, P., Alexander, B., Geng, L., Chi, X., Fan, S., Zhan, H., Kang, H., Zheng, G., Cheng, Y., Su, H., Liu, C., and Xie, Z.: Isotopic constraints on heterogeneous sulfate production in Beijing haze, Atmos. Chem. Phys., 18, 5515-5528, https://doi.org/10.5194/acp-18-5515-2018, 2018.

Jacob, D. J.: Heterogeneous chemistry and tropospheric ozone, Atmos. Environ., 34, 2131-2159, https://doi.org/10.1016/s1352-2310(99)00462-8, 2000.

Nenes, A., Pandis, S. N., and Pilinis, C.: ISORROPIA: A new thermodynamic equilibrium model for multiphase multicomponent inorganic aerosols, Aquat. Geochem., 4, 123-152, https://doi.org/10.1023/a:1009604003981, 1998.

Saylor, R., Edgerton, E., and Hartsell, B.: Linear regression techniques for use in the EC tracer method of secondary organic aerosol estimation, Atmos. Environ., 40, 7546-7556, https://doi.org/10.1016/j.atmosenv.2006.07.018, 2006.

Seinfeld, J. H., and Pandis, S. N.: Atmospheric chemistry and physics: From air pollution to climate change, second ed., John Wiley & Sons, New Jersey, 2006.

Stockwell, W. R., and Calvert, J. G.: The mechanism of the HO-SO_2 reaction, Atmos. Environ., 17, 2231-2235, https://doi.org/10.1016/0004-6981(83)90220-2, 1983.

Turpin, B. J., and Huntzicker, J. J.: Identification of secondary organic aerosol episodes and quantitation of primary and secondary organic aerosol concentrations during SCAQS, Atmos. Environ., 29, 3527-3544, https://doi.org/10.1016/1352-2310(94)00276-q, 1995.

Usher, C. R.: A laboratory study of the heterogeneous uptake and oxidation of sulfur dioxide on mineral dust particles, J. Geophys. Res., 107, https://doi.org/10.1029/2002JD002051, 2002.

Wang, K., Zhang, Y., Nenes, A., and Fountoukis, C.: Implementation of dust emission and chemistry into the Community Multiscale Air Quality modeling system and initial application to an Asian dust storm episode, Atmos. Chem. Phys., 12, 10209-

10237, https://doi.org/10.5194/acp-12-10209-2012, 2012.

Xing, L., Fu, T. M., Cao, J. J., Lee, S. C., Wang, G. H., Ho, K. F., Cheng, M. C., You, C. F., and Wang, T. J.: Seasonal and spatial variability of the OM/OC mass ratios and high regional correlation between oxalic acid and zinc in Chinese urban organic aerosols, Atmos. Chem. Phys., 13, 4307-4318, https://doi.org/10.5194/acp-13-4307-2013, 2013.

Zhang, R., Jing, J., Tao, J., Hsu, S. C., Wang, G., Cao, J., Lee, C. S. L., Zhu, L., Chen, Z., Zhao, Y., and Shen, Z.: Chemical characterization and source apportionment of $PM_{2.5}$ in Beijing: Seasonal perspective, Atmos. Chem. Phys., 13, 7053-7074, https://doi.org/10.5194/acp-13-7053-2013, 2013.

Zhang, X. Y., Gong, S. L., Shen, Z. X., Mei, F. M., Xi, X. X., Liu, L. C., Zhou, Z. J., Wang, D., Wang, Y. Q., and Cheng, Y.: Characterization of soil dust aerosol in China and its transport and distribution during 2001 ACE-Asia: 1. Network observations, J. Geophys. Res, 108, https://doi.org/10.1029/2002jd002632, 2003.

Zheng, B., Zhang, Q., Zhang, Y., He, K. B., Wang, K., Zheng, G. J., Duan, F. K., Ma, Y. L., and Kimoto, T.: Heterogeneous chemistry: a mechanism missing in current models to explain secondary inorganic aerosol formation during the January 2013 haze episode in North China, Atmos. Chem. Phys., 15, 2031-2049, https://doi.org/10.5194/acp-15-2031-2015, 2015.